International Journal of Hydrogen Energy 80 (2024) 1011–1020

Contents lists available at ScienceDirect

International Journal of Hydrogen Energy

journal homepage: www.elsevier.com/locate/he

Heat transfer to a catalytic multiphase dehydrogenation reactor

Miriam Willer [a,b], Patrick Preuster [d,e], Paolo Malgaretti [a], Jens Harting [a,f], Peter Wasserscheid [a,b,c,*]

[a] Forschungszentrum Jülich GmbH, Helmholtz-Institute Erlangen-Nürnberg for Renewable Energy (IEK 11), Cauerstraße 1, 91058, Erlangen, Germany
[b] Institute of Chemical Reaction Engineering, Friedrich-Alexander-Universität Erlangen-Nürnberg, Egerlandstraße 3, 91058, Erlangen, Germany
[c] Forschungszentrum Jülich GmbH, Institute for Sustainable Hydrogen Economy (INW), Am Brainergy Park 4, 52428, Jülich, Germany
[d] Rosenheim Technical University of Applied Sciences, Robert-Koch-Straße 28, 84489, Burghausen, Germany
[e] Fraunhofer IEG, Fraunhofer Research Institution for Energy Infrastructure and Geothermal Systems IEG, Am Hochschulcampus 1, 44801, Bochum, Germany
[f] Department of Chemical and Biological Engineering and Department of Physics, Friedrich-Alexander-Universität Erlangen-Nürnberg, Cauerstraße 1, 91058, Erlangen, Germany

ARTICLE INFO

Handling Editor: B Shabani

Keywords:
Heat transfer
Multiphase system
Dehydrogenation
Hydrogen storage
LOHC

ABSTRACT

The release of hydrogen from liquid organic hydrogen carriers (LOHC) takes place in an endothermal dehydrogenation reaction that is accompanied by a strong volume expansion. This leads to complex hydrodynamic properties that change drastically along the reactor axis due to product gas evolution. Consequently, heat transfer into the catalytic fixed-bed exhibits a pronounced local dependency. For a better understanding of such multiphase dehydrogenation systems, we have performed heat transport measurements in the presence of the chemical reaction, namely during the dehydrogenation of perhydro benzyltoluene (H12-BT) and perhydro dibenzyltoluene (H18-DBT). The results reveal that overall heat transfer coefficients show a clear local dependency on the axial coordinate. Moreover, the two carriers were found to differ significantly in their thermal behavior. Based on a global analysis, two main regimes can be distinguished in the dehydrogenation reactor: 1.) With the LOHC mixture being primarily in the liquid phase, heat transport is dominated and intensified by the hydrogen release; 2.) With an increasing proportion of LOHC vapor in the reactor, the heat transport is dominated by the gas phase, resulting in significantly lower thermal parameters.

1. Introduction

Understanding heat transport in fixed-bed reactors has been a subject of research for many years [1–3]. A sufficient description of the transport phenomena is a prerequisite for the successful design and optimization of reactors, especially for reactions with strong evolution or consumption of reaction heat. Those are typically carried out in multi-tubular reactors, which allow an effective temperature control due to their high specific surface area. Depending on the extent of endo- or exothermicity and the dimensional ratio of tube and particle ($d_R/d_P < 10$), these systems develop pronounced radial temperature profiles from the shell to the center of the catalyst bed. An exemplary profile for a heated packed tube is illustrated in Fig. 1. The strongest temperature change occurs on the inside of the tube and is, at the same time, challenging to quantify as various mechanisms take place simultaneously [3,4]. In the case of the one-dimensional pseudo-homogeneous continuum model (1DPH) all single phenomena of the complex transport process are lumped into one effective parameter: The overall heat transfer coefficient U [5–7]. It refers to the temperature difference between the inner wall ϑ_W and the radial average temperature ϑ_R of the catalyst bed. 1DPH is the simplest modeling approach, yet widely used for reactor design due to its high practicability and low computational effort [8,9]. It has been shown to be sufficient as long as thermal parameters are well estimated [10,11].

Literature offers thermal coefficients in fixed-bed systems for a multitude of different reaction conditions. The respective heat transport measurements have been typically performed in inert reference systems that represent the boundary conditions of the industrial reactor. In such studies, the fixed-bed has been replicated with inert particles, while model fluids were pushed through under defined thermal boundary conditions. Most studies concentrate on single-phase flows through packed beds [12–16]. The determination of thermal parameters in

* Corresponding author. Forschungszentrum Jülich GmbH, Helmholtz-Institute Erlangen-Nürnberg for Renewable Energy (IEK 11), Cauerstraße 1, 91058, Erlangen, Germany.
E-mail address: p.wasserscheid@fz-juelich.de (P. Wasserscheid).

https://doi.org/10.1016/j.ijhydene.2024.07.073
Received 10 May 2024; Received in revised form 27 June 2024; Accepted 6 July 2024

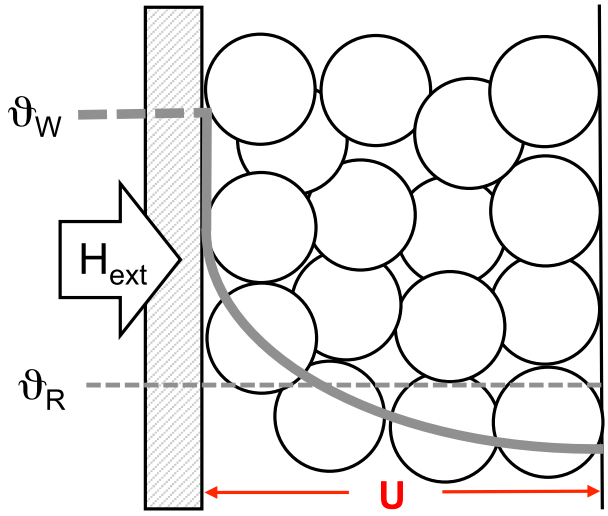

Fig. 1. Radial temperature profile for a heat transfer experiment with an endothermal reaction.

catalytic multiphase reactors is carried out with a simultaneous flow of gas and liquid phases. Most of these investigations relate to trickle bed reactors in which gaseous and liquid reactants flow downwards through the catalyst packing [17–20]. Hardly any correlations are available for fixed-beds that are operated in an upward direction [21,22]. A common characteristic of the available correlations is that the heat transport is typically assumed to be constant throughout the tube length. However, this can be insufficient and misleading, especially for multiphase reactions that are accompanied by gas formation and volume expansion. Although several studies have already highlighted the influence of the chemical reaction on the heat transport behavior in fixed-bed reactors, experimental determination in reactive systems is rarely carried out [23–25].

This publication deals with the endothermal dehydrogenation of the liquid organic hydrogen carriers perhydro benzyltoluene (H12-BT) and perhydro dibenzyltoluene (H18-DBT) in a tubular fixed-bed reactor. Due to the unique properties of the reaction, it has been found challenging to extract heat transfer coefficients from the literature that can be used confidently: The reaction requires a continuous supply of approximately 70 kJ mol_{H2}^{-1} [26] under typical reaction temperatures of 300 °C. Since the fully loaded carrier species stores a multiple of its liquid volume in hydrogen (1:670 at ambient conditions), the release of the gas is accompanied by an enormous volume expansion and a corresponding change of hydrodynamics in the reactor [27]. Additionally, a significant proportion of the liquid carrier phase evaporates throughout the reaction progress. In a preliminary study, we were able to show based on an equilibrium calculation that during dehydrogenation in a packed tubular reactor, up to 57 % of the H0-/H18-DBT species and 100% of H0-/H12-BT are in the vapor phase at the reactor exit. This leads to an additional impact on hydrodynamics, resulting in a shortening of the residence time and less favorable heat transport properties [28]. In order to operate the hydrogen release with the highest possible efficiency despite those challenging characteristics, research is being conducted on various reactor concepts, which intend to optimize the heat input [29–32]. So far, however, the conventional tubular reactor with vertical orientation and cocurrent upflow operation remains the most mature concept for larger scale applications [28,33], which is why heat transfer coefficients for the design of this configuration are of particular interest.

Preuster [34] has investigated the transport of heat in the dehydrogenation reactor by means of an inert experiment. The hydrodynamic conditions of the hydrogen release in upflow direction were simulated by a corresponding nitrogen gas flow at the bottom of the reactor. The resulting coefficients are in the range of 150–1400 W m^{-2} K^{-1} and show higher values, the stronger the gassing rate. Based on these findings, it was concluded that the heat input is intensified by the increased turbulence of rising bubbles. As the experiment was carried out in the absence of the chemical reaction and the inert gas flow was passed through the entire packed bed, the observed coefficients are assumed to be constant along the axial coordinate. However, this contradicts the aforementioned axial dependency of hydrodynamic conditions in the real system and the transferability to the technical reactor therefore remains limited.

Fig. 2 illustrates the presumed principle of the axially dependent heat transport in the dehydrogenation reactor. As the reaction itself contributes to continuously changing properties, we expect a feedback loop between heat transport and reaction. Starting from the pure liquid phase with a laminar flow character at the inlet of the catalyst bed, bubble formation may enhance the mixing on particle and bed scale and thereby support the transfer of a heat flow H_{ext}, increasing the temperature ϑ_R locally, which in turn leads to a stronger conversion X. This intrinsic amplification may prevail when LOHC is primarily in the liquid phase and only a small portion of hydrogen is released from the carrier. However, besides the effect of improved heat transport properties due to the bubble movement, hydrogen gas may also act as a thermal insulator because a higher gas content in the reactor increases the heat resistance. The self-promoting feedback loop would then be reversed into an impairment of the heat transport in the dehydrogenation reactor due to hydrogen release and evaporation of liquid reactants. Both cases of the cycle, however, may ultimately lead to an axial dependency of the heat transfer coefficient U = f(z), which can be analyzed in reactive systems only.

This contribution aims to advance the state of knowledge on heat transfer to catalytic multiphase dehydrogenation reactors. We introduce an experimental setup and an empirical model that allow us to investigate heat transfer coefficients and their dependency on axial position. The model uses data from heat transport experiments carried out in the presence of dehydrogenation reactions with H12-BT and H18-DBT and accordingly considers hydrogen formation as well as evaporation. This enables a comparison of both carrier systems and gives access to more reliable design parameters for the 1DPH modeling of continuous dehydrogenation reactors.

2. Experimental setup

Heat transport measurements were carried out during dehydrogenation of H12-BT and H18-DBT in a vertically oriented tubular reactor packed with the commercial Clariant EleMax-102D catalyst [35]. In order to adequately reflect the structural properties and d_R/d_P-ratio of an industrial reactor, the inner tube diameter (27.9 mm) was selected to mimic a technical tube bundle [33,36]. The catalyst zone had a length of 770 mm, which resulted in a reaction volume of approx. 470 mL. Fig. 3

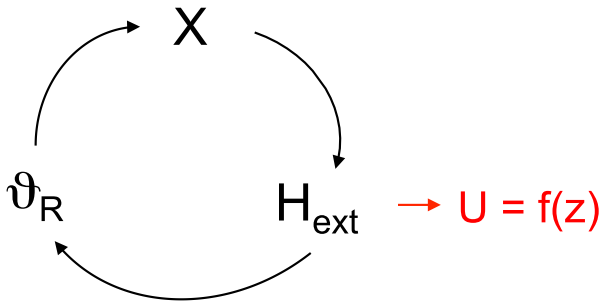

Fig. 2. Feedback loop between reaction progress X and heat transfer H_{ext}. Intrinsic amplification or impairment of heat transfer by hydrogen release leads to a local dependency of the heat transfer coefficient U on the axial coordinate z.

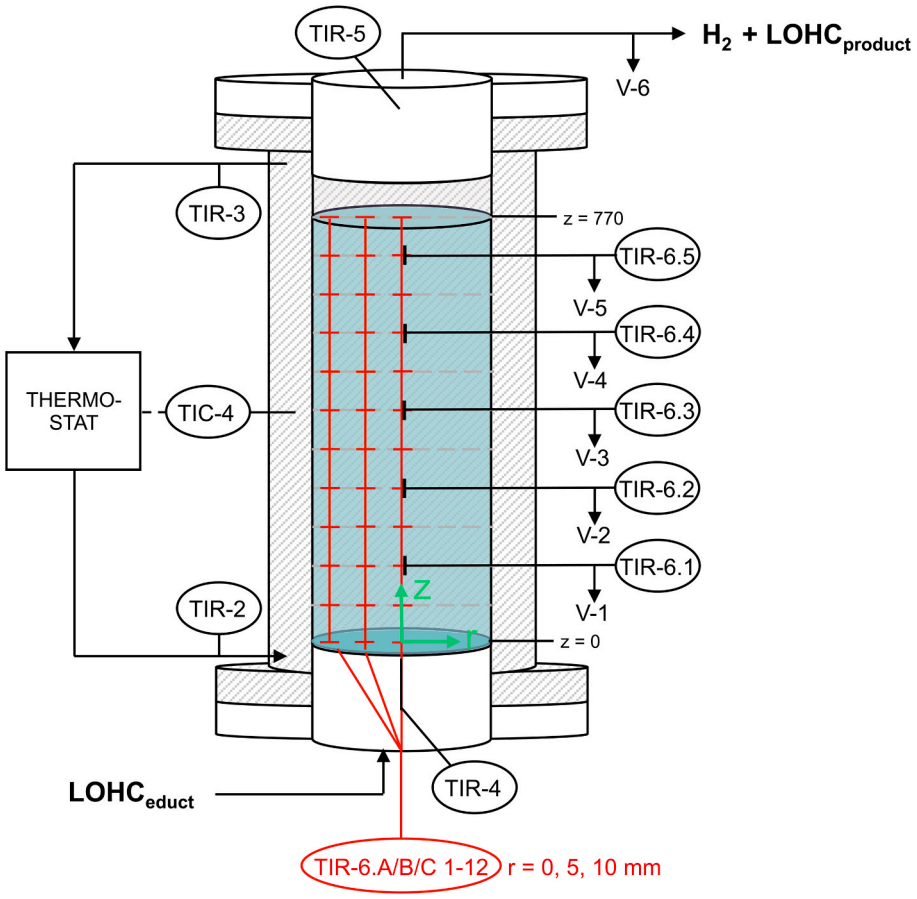

Fig. 3. Schematic sketch of the reactor module with sampling points (V-1–6), thermocouples (TIR-6.1-5) and fibre-optic temperature sensors (TIR-6.A/B/C.1-12).

shows a schematic sketch of the reactor module and its key elements. The shell side of the reactor was heated with a thermostat (Julabo forte HT60-M2-C.U.) and the temperature of the thermal oil was controlled via an external Pt-100 sensor (TIC-4). In order to maintain defined thermal boundary conditions for the experiments, the dimensions of the annular gap on the shell side were chosen according to the thermostat properties and expected heat consumption in the reactor. During the experiments the maximum temperature difference between inlet (TIR-2) and outlet (TIR-3) was monitored and always found below 1.6 K. The conditions in the shell were therefore considered to be isothermal. The wall temperature ϑ_W was taken as equal to the control point at TIC-4.

The determination of effective heat transfer coefficients in packed bed reactors is generally based on the measurement of radial temperature profiles, whereby a variety of different methods is known from the literature [37–40]. The selected technique should have as minimal influence as possible on the packing structure and, at the same time, provide the desired measurement resolution. Fiber-optic sensors combine several advantages with a high temporal and spatial resolution and relatively low invasiveness. The principle is based on the temperature measurement with fiber Bragg gratings, which are inserted at several discrete positions in a glass fiber [41,42]. We equipped the reactor with three fiber-optical sensors (TIR-6.A/B/C) SM800 from FiSens GmbH, each of which had 12 measuring points throughout the reactor axis.

This resulted in axial and radial temperature profiles $\vartheta = f(z, r)$ with a total of 36 measurement points across the packing. The data were recorded using a spectrometer (FiSpec from FiSens) and a lab-view based software (developed by the Fraunhofer Heinrich Hertz Institute). The positioning of the fibers at the radial coordinates r = 0, 5 and 10 mm was selected to minimize their impact on the packing properties. Fig. 4 shows the position of the sensors in a computer tomographic cross-sectional image (4-A) and a schematic sketch (4-B). Since the heat transport experiments were carried out in the presence of endothermic dehydrogenation reactions, the change of conversion over the reactor axis had to be determined in addition to temperature profiles. For this purpose, tap reactors are commonly used [43–45]. Our system was equipped with five equidistant sampling points along the length of the packing, from which reactant samples could be drawn by opening valves V-1 to V-5. At the outlet of each tapping point, a thermocouple (TIR-6.1-6.5) was inserted into the reaction zone and positioned just before the center (Fig. 4-C).

In addition to the purpose of validating the fiber-optic temperature measurement, the integration of the thermocouples is expected to have a positive effect on the sampling process: The lateral insertion loosens up the bed structure slightly, so that the sample is not exclusively taken from the wall region and thus more representative for the whole cross-sectional area.

The sampling was carried out in the stationary state of each operating point. The sample was first taken from the product line (V-6) and then from the reaction chamber against the main flow direction from the top (V-5) to the bottom (V-1) using glass bottles sealed to the outside. For each tapping point, the dead volume was first removed and then the actual sample was taken (V = 5 mL). The degree of dehydrogenation (DoD)[1] of each sample was determined using liquid phase analysis. Gas chromatography using an Agilent 8890 with a Rxi-17Sil MS column (L 30 m, d 250 μm) was applied to analyze H0-/H12-BT. The DoD of H0-/H18-DBT samples was determined by ^{1}H NMR spectroscopy in a Magritek Spinsolve 80. A detailed description of the respective methods

[1] The DoD is a measure of discharge of the carrier and corresponds to the molar ratio of released hydrogen to the maximum molar capacity.

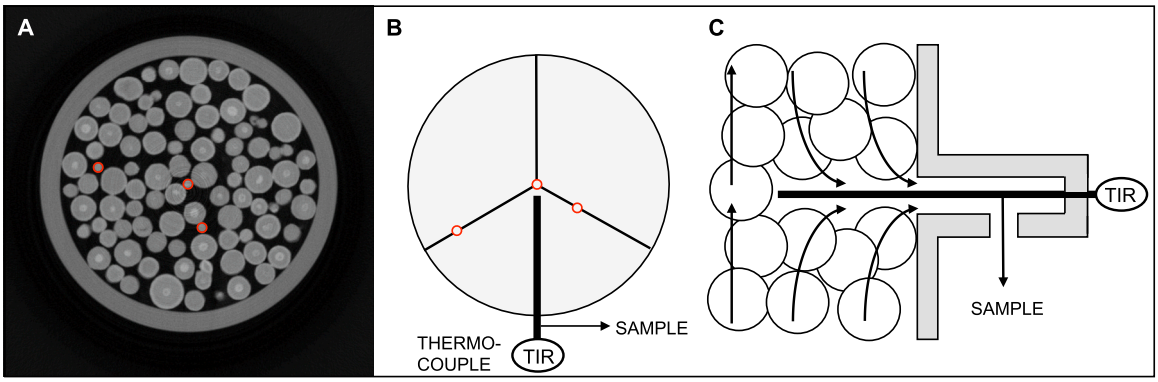

Fig. 4. (A) Radial positioning of fiber-optic sensors in a computer tomographic image, (B) cross-sectional sketch of the sensors and sampling point and (C) principle of sampling with expected flow behavior.

can be found in the literature [46,47].

Heat transport experiments were performed in the reactor module described above by carrying out dehydrogenation reactions with H12-BT [48] and H18-DBT [49]. A catalyst mass of 342.9 g was used for reactions with H12-BT, 342.4 g for the dehydrogenation of H18-DBT. The measurements covered a feed flow range of 5–25 mL min^{-1}, which corresponds to a liquid hourly space velocity (LHSV) of 0.6–3.2 h^{-1}. For each LHSV, the wall temperature ϑ_W was varied between 290 and 320 °C at a constant reaction pressure of 3 bar_a. A detailed description of the laboratory plant, catalyst preparation and execution of the experiments can be found in Ref. [28].

3. Methodology for the analysis of experimental data

The steady-state operating points of our dehydrogenation reactions were analyzed with an empirical model. Here, our methodological approach is subject to the main assumption of the 1DPH: A quasi-homogenous phase without fluid-to-particle heat and mass transfer resistances [50]. Axial dispersion and the generation of heat due to mechanical work were neglected as well. In order to investigate the aforementioned local dependency of heat transfer coefficients on the axial coordinate the vertical tube was modelled as a cascade of ideally mixed volume elements (VE). The position and number of the differential elements were defined by the axially distributed fiber-optic measuring grids, resulting in 11 VE with a height of 70 mm each.

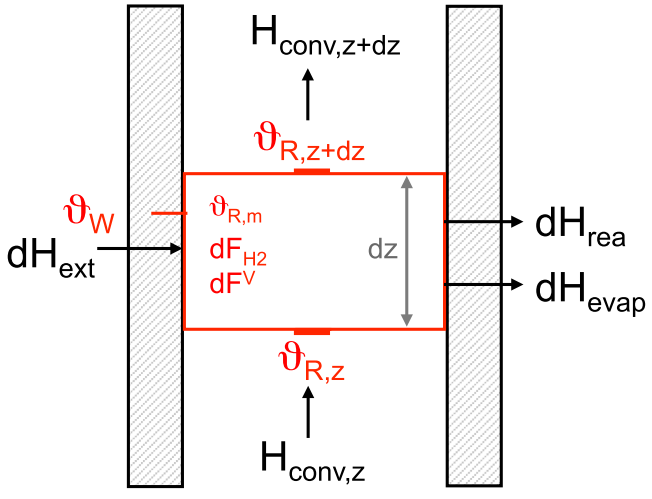

Fig. 5. Schematic sketch of a modeling element in the tubular reactor with the relevant variables. The heat balance includes the externally introduced heat flow, convective heat flow and the enthalpy consumption by reaction and evaporation.

Fig. 5 illustrates the modeling approach schematically.

At the upper and lower boundary of each differential element the mean reaction temperature $\vartheta_{R,z}$ per axial sensor position prevails. It results from circular averaging of a polynomial fit over the radial temperature measurement at r = 0, 5, 10 mm and the wall position. Within each VE, the reaction temperature was assumed to be the arithmetic mean value of the boundary temperatures. The amount of released hydrogen dF_{H2} was determined from the analysis of liquid samples over the packing length and is based on the differential change in the DoD. Under the assumption of steady-state operation, the external heat input per volume element dH_{ext} was determined as the sum of enthalpy change due to heat consumption by endothermal reaction dH_{rea}, evaporation of LOHC dH_{evap} and convective heat transport dH_{conv} (Eq. (1)).

$$dH_{ext} = dH_{rea} + dH_{evap} + dH_{conv} \tag{1}$$

The energy balance was subsequently solved for the local heat transfer coefficient U_{local} in the bed according to Equation (2). The resulting values refer to the radial temperature gradient $\Delta\vartheta_{rad}$ between the heated wall ϑ_W and the average temperature $\vartheta_{R,m}$ of each VE.

$$U_{local} = \frac{dH_{ext}}{dA\left(\vartheta_W - \vartheta_{R,m}\right)} = \frac{dH_{ext}}{dA\,\Delta\vartheta_{rad}} \tag{2}$$

Based on this approach, the global coefficient U_{global}, assuming a constant heat transfer throughout the reactor, can be calculated for a given data set by integration of the local dependency [51]:

$$U_{global} = \frac{1}{L}\int_1^L U_{local}\,dz \tag{3}$$

The energy demand of the endothermal reaction corresponds to the locally released hydrogen flow dF_{H2} multiplied by the molar reaction enthalpy:

$$dH_{rea} = dF_{H2}\cdot\Delta H_r^{H_2}\left(\vartheta_{R,m}, C_{p,H2}\right) \tag{4}$$

The molar reaction enthalpy is a function of temperature and isobaric heat capacity. The latter was determined using Kirchhoff's rule based on standard enthalpies according to Ref. [26]. In order to calculate the enthalpy consumption by evaporation, we assumed a vapor-liquid equilibrium (VLE) in the reactor and determined the molar rate dF^V of locally evaporated LOHC. The respective rate per species dF_i^V multiplied by the evaporation enthalpy Δh_i^{LV} corresponds to the consumed enthalpy according to Equation (5). Further details about the VLE calculation can be found in Ref. [28].

$$dH_{evap} = \sum_{i=1}^{2} dF_i^V\cdot\Delta h_i^{LV}\left(\vartheta_{R,m}\right) \tag{5}$$

Enthalpy change due to convective heat transport was deduced from the fluxes at the inlet and outlet of each volume element. Corresponding

flow rates of hydrogen, liquid and vapor LOHC resulted from the experimental hydrogen release in combination with the evaporation modelling. The respective mass flow rates M_i were multiplied by the isobaric heat capacity $C_{P,i}$ and the temperature at the boundary:

$$dH_{conv} = \left(M^{L}_{LOHC,z+dz}\, C^{L}_{P,LOHC} + M^{V}_{LOHC,z+dz}\, C^{V}_{P,LOHC} + M_{H2,z+dz}\, C_{P,H2}\right)\cdot T_{R,z+dz} - \left(M^{L}_{LOHC,z}\, C^{L}_{P,LOHC} + M^{V}_{LOHC,z}\, C^{V}_{P,LOHC} + M_{H2,z}\, C_{P,H2}\right)\cdot T_{R,z} \quad (6)$$

For the calculation of thermophysical and thermochemical properties, the reaction mixture, which in reality consists of several partially hydrogenated species [52], was approximated as a mixture of hydrogen-lean (H0-BT/H0-DBT) and hydrogen-rich (H12-BT/H18-DBT) compounds. The respective properties then resulted from linear interpolation of the pure substance properties based on correlations given in the literature [26]. In addition, the heat capacity of the vapor phase $C^{V}_{P,LOHC}$ was estimated using the group contribution method according to Benson by using the NIST Chemistry WebBook [53]. The effect of higher and lower boiling by-products in the reaction mixture were not considered significant for the reactions carried out [46,54]. These species were therefore not included in the model.

In addition to heat transfer coefficients, the presented model determines local flow rates of the liquid and gaseous phase in the reaction zone. The volume flow of the liquid phase f_L results from the sum of mass flows of the respective LOHC species divided by the average density:

$$f_L = \frac{\sum_{i=1}^{2} M^{L}_{i}}{\rho^{L}_{LOHC}} \quad (7)$$

The volume flow rates of the gaseous phase then correspond to the sum of evaporated LOHC species and the accumulated hydrogen flow:

$$f_G = \frac{\sum_{i=1}^{2} M^{V}_{i}}{\rho^{V}_{LOHC}} + F_{H2} \bullet V_m \quad (8)$$

4. Results and discussion

4.1. Temperature profiles and local heat transfer

According to the methodology presented, the local heat transport characteristics in the reactor were analyzed based on measured temperature and concentration changes. Fig. 6 shows the resulting profiles for dehydrogenation reactions with H18-DBT (A) and H12-BT (B) under variation of LHSV from 0.6 to 3.2 h^{-1} at a pressure level of 3 bar_a and a wall-side temperature of 320 °C. The 1D axial temperature profiles start at inlet temperatures between 293 and 302 °C and show typical courses for a polytropic reaction control. However, the detailed temperature behavior of the two LOHC systems is very different despite comparable boundary conditions: While H18-DBT (Fig. 6-A) shows continuously rising profiles, H12-BT (Fig. 6-B) exhibits pronounced temperature drops shortly after entering the reaction zone (z = 70–140 mm) with a maximum decrease of 15 K at 0.6 h^{-1}. At the same time, the DoD profiles indicating the reaction progress show lower values for H12-BT compared to H18-DBT in this part of the reactor. Table 1 compares the molar hydrogen rate that corresponds to the respective change of DoD at a LHSV of 0.6 h^{-1} within the first 140 mm of the reaction zone. In the case of H18-DBT, 1.5 10^{-3} mol s^{-1} were produced, whereas only two-thirds of this were released during the dehydrogenation of H12-BT (1.0 10^{-3} mol s^{-1}).

Consequently, the clearly different temperature behavior of H12-BT cannot be caused by a stronger cooling effect of the endothermic reaction. Since H12-BT has a much higher vapor pressure, the carrier evaporates more strongly under the same conditions, which leads to a higher heat transport resistance due to the changed phase distribution towards a higher proportion of the gaseous phase [28]. Based on the profiles indicating the change of temperature and reaction progress, heat transfer coefficients were determined. Beforehand, the respective profiles underwent a fitting, which is shown as black lines in the diagrams. Small fluctuations of the local temperature measurement, which cannot be attributed to physical phenomena, were compensated by a Savitzky-Golay filter in MATLAB. The fitting was carried out single-stage in the case of monotonically increasing temperature profiles and multiple-stage in the case of an observed cooling effect. DoD profiles indicating the reaction progress were fitted with an exponential function in order to extend the 7 datapoints to 12 values throughout the reactor length.

Local heat transfer coefficients U_{local} for both carrier systems are shown in the right diagrams of Fig. 6-A and 6-B. The parameters are generally high at the beginning of the tube, where a lot of hydrogen is released and they decrease steadily towards the end of the reaction zone. H18-DBT shows high coefficients between 710 and 920 W m^{-2} K^{-1}, which drop to values of 80–340 W m^{-2} K^{-1}. The observed courses show a clear local dependency, which is particularly pronounced for low LHSV rates. In contrast, thermal parameters of H12-BT are lower in the first volume element (290–600 W m^{-2} K^{-1}) and decrease faster to values of 100–210 W m^{-2} K^{-1}. This observation seems to be consistent with the presumed feedback loop of reaction and heat transport in the dehydrogenation reactor: The intrinsic amplification can appear when LOHC is primarily in the liquid phase, which is the case at the tube inlet and generally more pronounced for H18-DBT due to its lower vapor pressure. H12-BT in contrast tends to evaporate more quickly and therefore reaches the unfavorable condition with an intrinsic impairment of heat transfer earlier, resulting in a faster drop of thermal parameters.

In addition to the qualitative consideration, the axial dependency of the heat transfer coefficient can be expressed quantitatively using the normalized variance NV. It is defined as a measure of variation of the local coefficient U_{local} relative to its mean value $\overline{U_{local}}$:

$$NV = \frac{\sqrt{\frac{1}{n-1}\sum_{i=1}^{n}\left(U_{local,i} - \overline{U_{local}}\right)^2}}{\overline{U_{local}}} \quad (9)$$

Table 2 shows the corresponding variance data for both carriers in the respective LHSV range. It includes the mean values $\overline{NV}$ of the profiles in the range of the investigated wall temperatures between 290 and 320 °C. The values support the observation of a particularly pronounced axial dependency for dehydrogenation of H18-DBT at low LHSV ($\overline{NV}$ = 0.86) and smaller changes at higher reactant rates. In the case of H12-BT, the normalized variance in the entire LHSV range is on a medium level of 0.55–0.68 without a clear connection to LHSV.

4.2. Global heat transfer

In order to further investigate the heat transfer behavior in dependency on heating temperature, a global analysis – referring to the average of the tube – is carried out as follows. Fig. 7-A shows the operating fields for both carriers, namely the overall achieved DoD as a function of LHSV and wall temperature [28].

Under these operating conditions, H18-DBT covers a DoD range of 0.21–0.84 and H12-BT from 0.34 to 0.88. With increasing wall temperature, both carriers reach a higher DoD - as expected from thermodynamics and kinetics. The global heat transfer coefficients U_{global} (Fig. 7-B) for the operating data were obtained by integration of the local heat transfer parameters. Firstly, the plot reveals that the global coefficients of the two carriers differ in their relative position from each other. U_{global} of H18-DBT is in the range of 253–563 W m^{-2} K^{-1}, while for H12-BT considerably lower values of 136–365 W m^{-2} K^{-1} are obtained. In addition, a different temperature behavior can be observed: Global heat transfer during dehydrogenation of H18-DBT basically increases with higher temperature, although at higher temperatures,

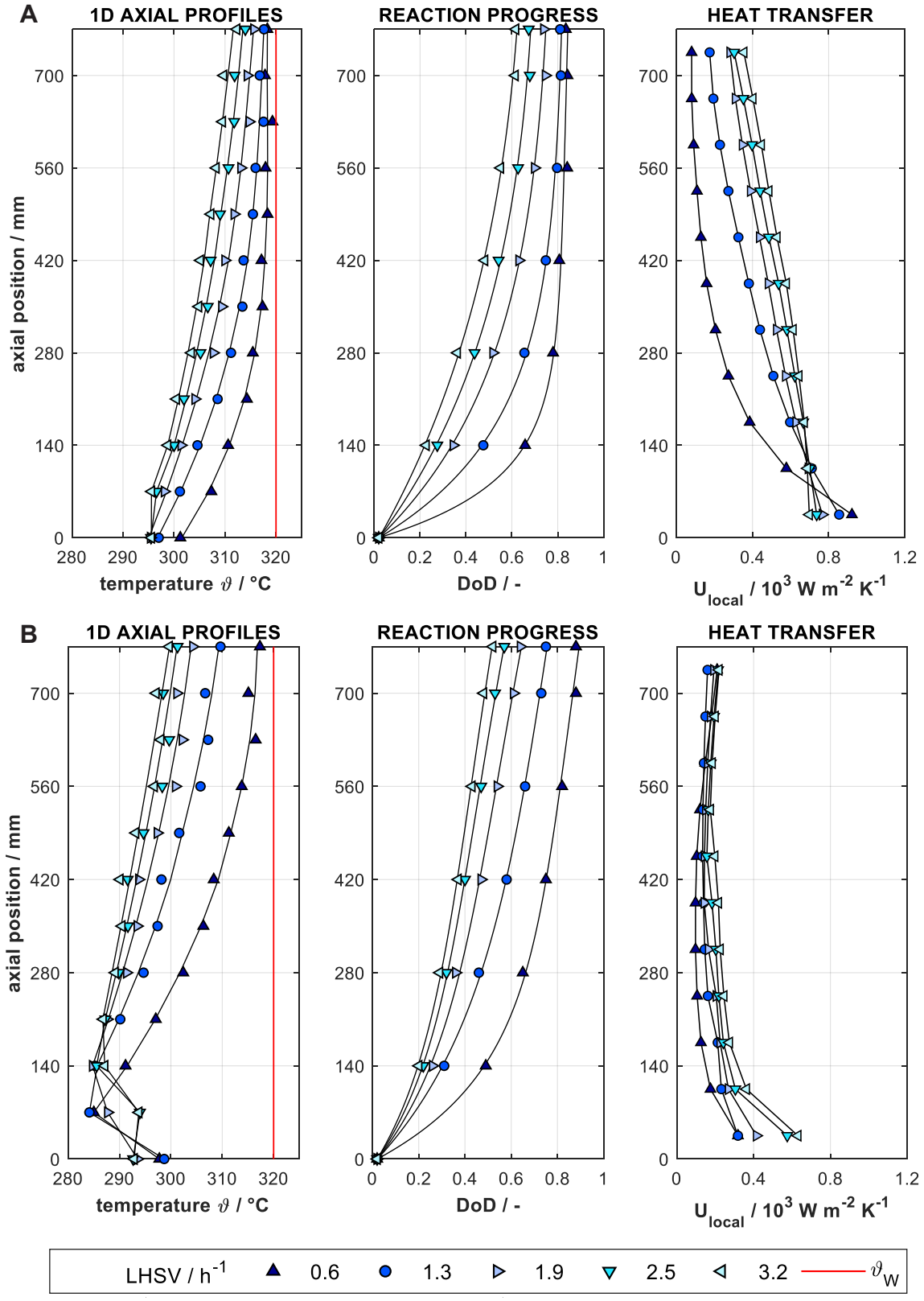

Fig. 6. Multiplot with 1D axial temperature profiles, DoD profiles and local coefficients for H18-DBT (A) and H12-BT (B) at a reaction pressure of 3 bar_a, heating temperature ϑ_W of 320 °C and a reactant flow rate LHSV between 0.6 and 3.2 h^{-1}. $DoD_{in} = 0.02$.

Table 1
Released molar hydrogen flow within the first 140 mm of the reaction zone for H12-BT versus H18-DBT. LHSV = 0.6 h^{-1}, ϑ_W = 320 °C.

Reactant	f_{H2} / mol s^{-1}
H12-BT	1.0 10^{-3}
H18-DBT	1.5 10^{-3}

Table 2
Mean normalized variance $\overline{NV}$ of local heat transfer coefficients per reactant and LHSV rate in the temperature range of ϑ_W = 290–320 °C.

LHSV / h^{-1}	0.6	1.3	1.9	2.5	3.2
$\overline{NV}$ | ϑ_W = 290–320 °C					
H18-DBT	0.86	0.46	0.33	0.26	0.21
H12-BT	0.55	0.56	0.66	0.68	0.64

310–320 °C, it seems to reach a plateau. In contrast, U_{global} for dehydrogenation of H12-BT decreases upon increasing the wall temperature, with a clear trend towards lower values at higher wall temperatures.

This surprising behavior can be explained by the relation between the total heat consumption H_{ext} and the radial temperature difference $\Delta\vartheta_{rad}$ from the heated wall to the reaction chamber (see Fig. 8). Note, that the globally consumed amount of heat and radial temperature difference are only used to explain the phenomenon at this point and not to calculate the global transfer parameters. Firstly, Fig. 8 shows that $\Delta\vartheta_{rad}$ during dehydrogenation of H12-BT is significantly higher compared to H18-DBT despite a similar heat consumption. This contributes to the fact that U_{global} is generally lower for H12-BT. Furthermore, the ratio of H_{ext} to $\Delta\vartheta_{rad}$ shows a non-linear behavior with increasing wall temperature. In the case of H18-DBT, the relation increases for the majority of operation points with higher ϑ_W, while it decreases for H12-BT. Consequently, the heat transport coefficients during dehydrogenation of the two carriers show an opposite dependence on ϑ_W. It is interesting to note that the dependence of U_{global} on ϑ_W is very sensitive to the chemical compounds involved. Our data therefore show that changing the carrier, as here from the BT-based to the DBT-based LOHC system, leads to a large difference in the heat transport properties and can therefore significantly change the boundary conditions for the design and optimization of the reactor.

The temperature behavior of the global heat transfer coefficient for both carrier systems can be attributed to different hydrodynamic regimes in the fixed-bed. Fig. 9-A shows the dependence of U_{global} on the average evaporated mass fraction of the liquid carrier. The latter results from the evaporation calculation in the empirical model and is therefore subject to the assumption of a vapor-liquid equilibrium. In order to determine the given mean value, the vapor fractions over the 11 axial VE

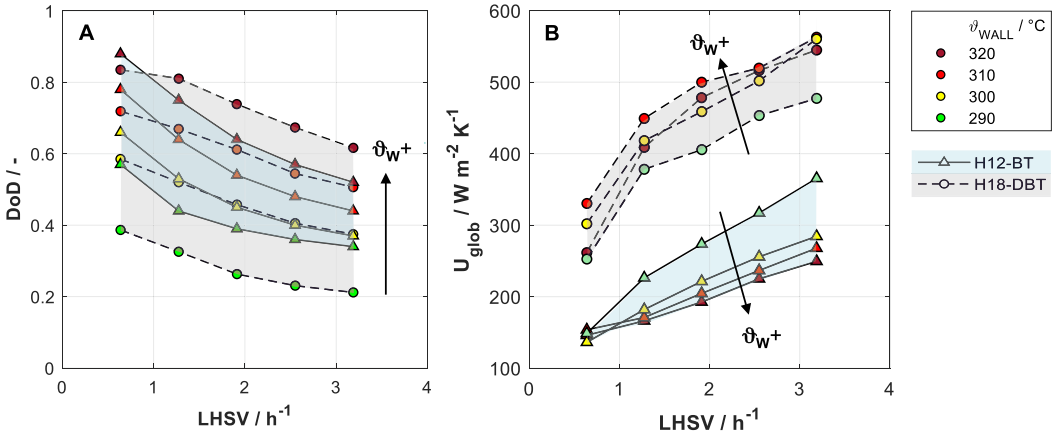

Fig. 7. Global comparison of the dehydrogenation of H12-BT (blue) and H18-DBT (grey) at a reaction pressure of 3 bar_a. (A) Degree of dehydrogenation according to Ref. [28] and (B) global heat transfer coefficients U_{global} versus LHSV (0.6–3.2 h^{-1}) for different wall temperatures. Global coefficients originate from the integration of local values U_{local} = f(z). DoD_{in} = 0.02. (For interpretation of the references to colour in this figure legend, the reader is referred to the Web version of this article.)

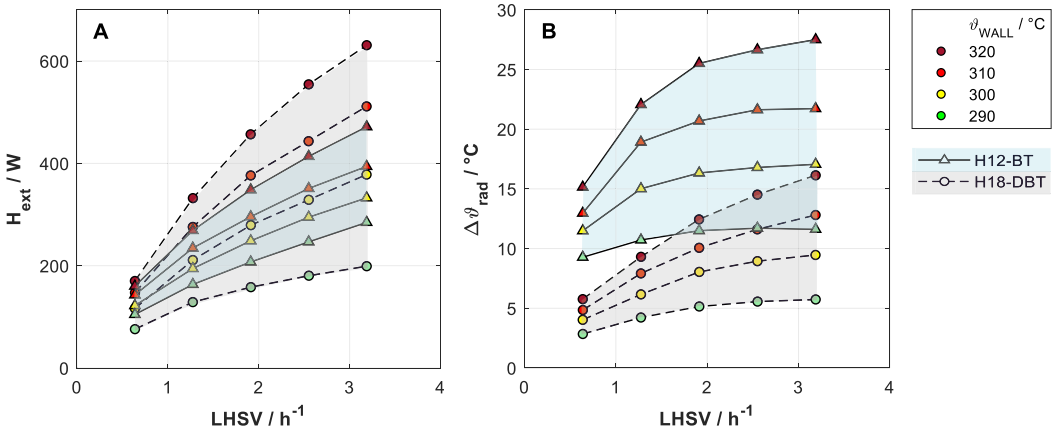

Fig. 8. Global assessment of (A) heat consumption and (B) mean radial temperature difference between heated wall and average reaction temperature over LHSV from 0.6 to 3.2 h^{-1}. Blue areas indicate results for H12-BT and grey areas for H18-DBT, respectively. Reaction conditions: p = 3 bar_a, DoD_{in} = 0.02. (For interpretation of the references to colour in this figure legend, the reader is referred to the Web version of this article.)

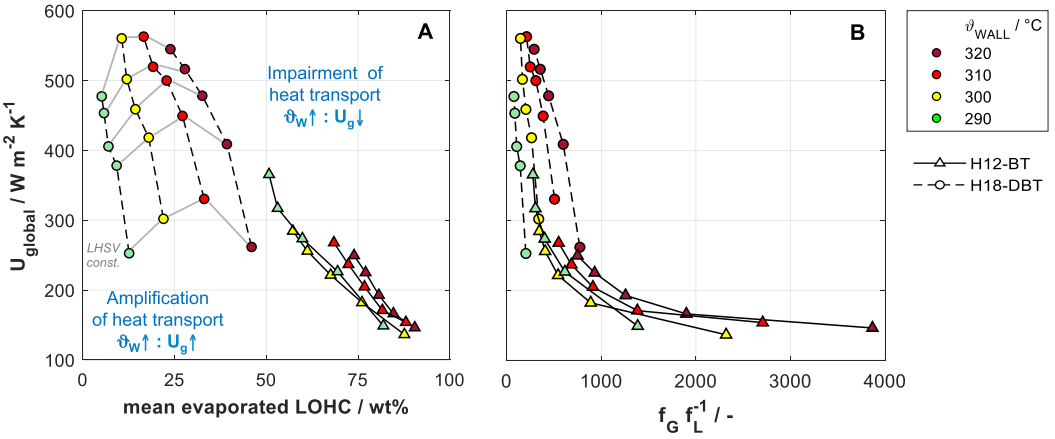

Fig. 9. Global heat transfer coefficients over (A) the average fraction of evaporated LOHC and (B) the ratio of average volume flow rates of gaseous and liquid phases in the reactor. Operating points with constant LHSV in Fig. 9-A are indicated with interpolated lines in grey.

were averaged. The figure reveals that the values of U_{global} of the two carriers are located in two different areas of the plot. Dehydrogenation of H18-DBT generally takes place in the range of lower mean vapor contents (5–46 %), whereas for H12-BT it occurs at higher fractions (>50 %). If, starting from the lowest vapor content, the wall temperature is increased at constant LHSV, U_{global} increases, which corresponds to the release rate of the reaction. In this regime, the heat input into the fixed-bed reactor is therefore dominated and amplified by the reaction. Towards a higher vapor content, however, this trend seems to reach a plateau and turns into the opposite behavior. From this turning point, which is between 20 and 40 wt% mean evaporated LOHC depending on the LHSV, the hydrodynamic situation in the reactor appears to change to a regime in which the heat input is no longer amplified by generated hydrogen, but rather dominated by the increased heat transport resistance of the gas phase. This is reflected by a drop in U_{global} as ϑ_W and, consequently, the vapor content increases. Global heat transfer coefficients during dehydrogenation of H12-BT correspond to this behavior over the entire operating window with an average vapor content of 50–90 wt%.

The identified regimes can be physically explained by the ratio of the volume flows between gas and liquid phase. In Fig. 9-B, the global heat transfer coefficient is plotted against the ratio of the axially averaged volume flows prevailing in the reactor. Note, that the gas volume flow f_G corresponds to the sum of hydrogen gas and evaporated LOHC. The plot shows that the magnitude of U_{global} correlates clearly with the respective ratio. If the ratio is low, there is a sufficient proportion of the LOHC system in the liquid phase, where released hydrogen bubbles presumably contribute to increased mixing. The heat input then proceeds mainly via forced convection and is favored by the bubble generation according to the principle of intrinsic amplification. The higher the ratio of gas to liquid volume, the more the reaction takes place under gas phase conditions, which leads to an increased thermal resistance and thereby an impairment of heat transport. Mechanistically, heat transport under these conditions can merely proceed via point contacts of the catalyst particles and is therefore strongly reduced compared to the transport processes in the bubbly liquid phase.

Fig. 9-B confirms that U_{global} in the reactive system is not only dependent on the volume flow ratio, but also on the wall temperature. This is expressed by the fact that the functional relationship between heat supply and volume flow ratio is close to a series of four isotherms (ϑ_W = const.). Up to a ratio of approx. 1000, the resulting coefficients are clearly dependent on the respective wall temperature; at higher ratios, however, the coefficients approach an almost constant level of approx. 160 W m^{-2} K^{-1}.

The data from the results section of this publication are also available via Zenodo [55].

5. Conclusion

In this contribution, heat transfer to a tubular fixed-bed reactor for the dehydrogenation of liquid organic hydrogen carriers was investigated. The endothermal reaction requires 70 kJ mol^{-1} hydrogen and is accompanied by a strong volume expansion and evaporation of liquid reactants, which leads to complex and constantly changing hydrodynamic conditions along the axis of the reactor. As the phase distribution changes accordingly from a pure liquid over a multiphase system to an almost pure gas phase, the heat transport in the packed bed is expected to have a local dependency throughout the length of the tube. These conditions are not adequately represented in available literature correlations. In order to determine heat transfer coefficients that can be used confidently for the design of technical dehydrogenation reactors, we have carried out heat transport experiments under reactive conditions. Dehydrogenation reactions were performed with H12-BT and H18-DBT under variation of reactant flow and heating temperature in a single tubular reactor that was equipped with a high-resolution temperature measurement system and various sampling points throughout the length of the packing. The experimental data was subsequently analyzed using a model that regards heat consumption by reaction, convection and evaporation in the reactor, resulting in overall heat transfer coefficients that correspond to the 1D pseudo homogeneous modeling approach. The local analysis has revealed a clear dependency of the heat transfer on the axial coordinate for both LOHC systems with high values of the local heat transfer coefficient at the entrance and lower towards the end of the reactor. Beyond this, however, the two carriers differ significantly in their heat transport behavior: H18-DBT shows high values of the local heat transfer coefficient up to 920 W m^{-2} K^{-1} at the inlet, which drop steadily to values of 80–340 W m^{-2} K^{-1} along the reactor axis. The parameters of H12-BT, in contrast, start at lower values of max. 600 W m^{-2} K^{-1} and decrease quickly to 100–210 W m^{-2} K^{-1} at equal boundary conditions. This is also reflected in the fact that H12-BT dehydrogenation generally reaches lower reaction temperatures in the catalyst packing. However, a comparison of the released hydrogen flows shows that this is not caused by a stronger cooling effect due to the endothermal reaction. Due to its higher vapor pressure, the carrier is primarily present in the gaseous phase at comparable conditions, which leads to higher heat transport resistances. These local observations were confirmed by a global analysis: The respective mean heat transfer coefficients for H18-DBT are in the range of 253–563 W m^{-2} K^{-1}, whereas coefficients for H12-BT are considerably lower at 136–365 W m^{-2} K^{-1}. The global coefficients for both carriers further show a distinct dependency on the wall temperature, which can be explained by the proportion of evaporated LOHC compounds in the reactor. Dehydrogenation of H18-DBT predominantly takes place in the range of low

average vapor contents, where global parameters increase with higher heating temperatures. In this area of low gas-to-liquid volume ratios, the bubbles of the released hydrogen may contribute to an intensified mixing and thereby amplify the heat transport. With further increasing vapor fractions between 20 and 40 wt%, however, this regime seems to transition to a state, where heat transport is dominated by the gas phase due to the higher heat transport resistance. As a result, heat transport is hindered by the hydrogen release, leading to a negative dependency of global coefficients on the wall temperature. This regime was clearly observed at vapor fractions above 40 wt%, which are present at dehydrogenation reactions of H12-BT for all operation conditions. Particularly for the continuous dehydrogenation of H12-BT, future research should therefore focus on reactor concepts that limit the accumulation of hydrogen and thus the evaporation of the carrier. An interesting option for this is the use of membrane reactors [31,56]. The observations of this study conclusively demonstrate that heat transport to multiphase reactions with volume expansion is strongly influenced by the chemical reaction. A determination of thermal parameters in the presence of the reaction is therefore a prerequisite to obtain robust modeling parameters for reactor design and upscaling.

CRediT authorship contribution statement

Miriam Willer: Writing – original draft, Methodology, Investigation, Conceptualization, Formal analysis, Visualization. **Patrick Preuster:** Writing – review & editing, Supervision, Methodology, Conceptualization. **Paolo Malgaretti:** Writing – review & editing, Methodology. **Jens Harting:** Writing – review & editing. **Peter Wasserscheid:** Writing – review & editing, Supervision, Methodology, Funding acquisition, Conceptualization.

Declaration of competing interest

Peter Wasserscheid is founder and minority share holder of the company Hydrogenious LOHC technologies (www.hydrogenious.net) that offers commercially hydrogen storage systems based on the LOHC technology.

There is no conflict of interest to declare with regard to the specific scientific results reported in this paper.

Nomenclature

Abbreviations

1DPH	onedimensional pseudo-homogeneous model
H0-BT	benzyltoluene
H12-BT	perhydro benzyltoluene
H0-DBT	dibenzyltoluene
H18-DBT	perhydro dibenzyltoluene
LOHC	liquid organic hydrogen carrier
VE	volume element

Symbols

A	heat transfer area [m^2]
C_P	isobaric heat capacity [J kg^{-1} K^{-1}]
d	diameter [m]
DoD	degree of dehydrogenation [−]
F	molar flow rate [mol s^{-1}]
f	volumetric flow rate [mol^3 s^{-1}]
Δh^{LV}	molar vaporisation enthalpy [J mol^{-1}]
H_{conv}	enthalpy change due to convective heat transport [W]
H_{evap}	enthalpy change due to evaporation [W]
H_{ext}	externally introduced enthalpy [W]
H_{rea}	enthalpy change due to reaction [W]
ΔH_r	reaction enthalpy [J mol^{-1}]
L	length of reaction zone [m]
LHSV	liquid hourly space velocity [h^{-1}]
M	mass flow rate [kg s^{-1}]
NV	normalized variance [−]
p	pressure [P]
r	radial coordinate [m]
ρ	density [kg m^{-3}]
T	temperature [K]
ϑ	temperature [°C]
U	overall heat transfer coefficient [W m^{-2} K^{-1}]
X	conversion [−]
z	axial coordinate [m]

Indices

G	gaseous
global	global value, referring to the average of the reactor
H2	hydrogen
i	index of a given chemical component
in	inlet of reaction zone
L	liquid
local	local value, referring to one volume element of the reactor
m	average
r	radial coordinate
R	related to the reaction zone
out	outlet of reaction zone
P	particle
z	axial coordinate
V	vapor
W	condition at the reactor wall

References

[1] Achenbach E. Heat and flow characteristics of packed beds. Exp Therm Fluid Sci 1995:17–27. https://doi.org/10.1016/0894-1777(94)00077-L.

[2] Winterberg M, Tsotsas E, Krischke A, Vortmeyer D. A simple and coherent set of coefficients for modelling of heat and mass transport with and without chemical reaction in tubes filled with spheres. Chem Eng Sci 2000:967–79. https://doi.org/10.1016/S0009-2509(99)00379-6.

[3] Dixon AG. Fixed bed catalytic reactor modelling—the radial heat transfer problem. Can J Chem Eng 2012;90:507–27. https://doi.org/10.1002/cjce.21630.

[4] Kulyk N, Berger D, Smith A-S, Harting J. Catalytic flow with a coupled finite difference — lattice Boltzmann scheme. Comput Phys Commun 2020;256:107443. https://doi.org/10.1016/j.cpc.2020.107443.

[5] Dixon AG. Thermal resistance models of packed-bed effective heat transfer parameters. AIChE J 1985;31:826–34. https://doi.org/10.1002/aic.690310519.

[6] Jess A, Wasserscheid P. Chemical technology. Weinheim, Germany: Wiley-VCH Verlag GmbH & Co. KGaA; 2013.

[7] Horn R. Reaktoren für Fluid-Feststoff-Reaktionen: Festbettreaktoren. In: Reschetilowski W, editor. Handbuch Chemische Reaktoren. Berlin, Heidelberg: Springer Berlin Heidelberg; 2020. p. 1–70.

[8] Adler R. Stand der Simulation von heterogen-gaskatalytischen Reaktionsabläufen in Festbettrohrreaktoren - Teil 1. Chem Ing Tech 2000:555–64. https://doi.org/10.1002/1522-2640(200006)72:6<555:AID-CITE555>3.0.CO;2-%23.

[9] Adler R. Stand der Simulation von heterogen-gaskatalytischen Reaktionsabläufen in Festbettrohrreaktoren - Teil 2. Chem Ing Tech 2000:688–99. https://doi.org/10.1002/1522-2640(200007)72:7<688:AID-CITE688>3.0.CO;2-4.

[10] Taulamet MJ, Mariani NJ, Barreto GF, Martínez OM. Estimation of overall heat transfer coefficients in packed beds with cocurrent downflow of gas and liquid. Fuel 2014;138:176–82. https://doi.org/10.1016/j.fuel.2014.07.064.

[11] Dixon AG. An improved equation for the overall heat transfer coefficient in packed beds. Chem Eng Process 1996:323–31. https://doi.org/10.1016/0255-2701(96)80012-2.

[12] Borkink JGH, Westerterp KR. Influence of tube and particle diameter on heat transport in packed beds. AIChE J 1992;38:703–15. https://doi.org/10.1002/aic.690380507.

[13] Bey O, Eigenberger G. Gas flow and heat transfer through catalyst filled tubes. Int J Therm Sci 2001:152–64. https://doi.org/10.1016/S1290-0729(00)01204-7.

[14] Martin H, Nilles M. Radiale Wärmeleitung in durchströmten Schüttungsrohren. Chem Ing Tech 1993;12:1468–77. https://doi.org/10.1002/cite.330651206.

[15] Seidel H-P. Untersuchungen zum Wärmetransport in Füllkörpersäulen. Chem Ing Tech 1965;37:1125–32. https://doi.org/10.1002/cite.330371108.

[16] Dixon A, DiCostanzo MA, Soucy BA. Fluid-phase radial transport in packed beds of low tube-to-particle diameter ratio. Int J Heat Mass Tran 1984;27:1701–13. https://doi.org/10.1016/0017-9310(84)90153-4.

[17] Specchia V, Baldi G. Heat transfer in trickle-bed reactors. Chem Eng Commun 1979;3:483–99. https://doi.org/10.1080/00986447908935880.

[18] Mariani NJ, Barreto GF. Evaluation of heat transfer parameters in packed beds with cocurrent downflow of liquid and gas. Chem Eng Sci 2001;56:5995–6001. https://doi.org/10.1016/S0009-2509(01)00225-1.

[19] Borremans D, Rode S, Carré P, Wild G. The influence of periodic operation on the effective radial thermal conductivity in trickle bed reactors. Can J Chem Eng 2003; 81:795–801. https://doi.org/10.1002/cjce.5450810361.
[20] Taulamet MJ, Mariani NJ, Barreto GF, Martínez OM. Prediction of thermal behavior of trickle bed reactors: the effect of the pellet shape and size. Fuel 2017; 202:631–40. https://doi.org/10.1016/j.fuel.2017.04.031.
[21] Larachi F, Belfares L, Iliuta I, Grandjean BPA. Heat and mass transfer in cocurrent gas−liquid packed beds. Analysis, recommendations, and new correlations. Ind Eng Chem Res 2003;42:222–42. https://doi.org/10.1021/ie020416g.
[22] Taulamet MJ, Mariani NJ, Barreto GF. A critical review on heat transfer in trickle bed reactors. Rev Chem Eng 2015:97–118. https://doi.org/10.1515/revce-2014-0050.
[23] Haidegger E. Der radiale Wärmetransport in wandgekühlten katalytischen Festbettreaktoren mit exothermer chemischer Reaktion. Dissertation: Technische Universität München; 1990.
[24] Ooms G, Groen G, de Graag DP, Ballintijn F. On turbulent pipe flow with heat transfer and chemical reaction. Chem Eng Sci 1978;33:357–63. https://doi.org/10.1016/0009-2509(78)80093-1.
[25] Golding JA. Conversions and temperature rises in a tubular reactor with heat transfer at the wall-exothermic reaction. AIChE J 1981;27:1026–8. https://doi.org/10.1002/aic.690270623.
[26] Müller K, Stark K, Emel'yanenko VN, Varfolomeev MA, Zaitsau DH, Shoifet E, Schick C, Verevkin SP, Arlt W. Liquid organic hydrogen carriers: thermophysical and thermochemical studies of benzyl- and dibenzyl-toluene derivatives. Ind Eng Chem Res 2015;54:7967–76. https://doi.org/10.1021/acs.iecr.5b01840.
[27] Heublein N, Stelzner M, Sattelmayer T. Hydrogen storage using liquid organic carriers: equilibrium simulation and dehydrogenation reactor design. Int J Hydrogen Energy 2020;45:24902–16. https://doi.org/10.1016/j.ijhydene.2020.04.274.
[28] Willer M, Preuster P, Geißelbrecht M, Wasserscheid P. Continuous dehydrogenation of perhydro benzyltoluene and perhydro dibenzyltoluene in a packed bed vertical tubular reactor – the role of LOHC evaporation. Int J Hydrogen Energy 2024;57:1513–23. https://doi.org/10.1016/j.ijhydene.2024.01.031.
[29] Peters W, Eypasch M, Frank T, Schwerdtfeger J, Körner C, Bösmann A, Wasserscheid P. Efficient hydrogen release from perhydro-N-ethylcarbazole using catalyst-coated metallic structures produced by selective electron beam melting. Energy Environ Sci 2015;8:641–9. https://doi.org/10.1039/C4EE03461A.
[30] Solymosi T, Auer F, Dürr S, Preuster P, Wasserscheid P. Catalytically activated stainless steel plates for the dehydrogenation of perhydro dibenzyltoluene. Int J Hydrogen Energy 2021;46:34797–806. https://doi.org/10.1016/j.ijhydene.2021.08.040.
[31] Wunsch A, Mohr M, Pfeifer P. Intensified LOHC-dehydrogenation using multi-stage microstructures and Pd-based membranes. Membranes 2018;8. https://doi.org/10.3390/membranes8040112.
[32] Kadar J, Gackstatter F, Ortner F, Wagner L, Willer M, Preuster P, Wasserscheid P, Geißelbrecht M. Boosting power density of hydrogen release from LOHC systems by an inverted fixed-bed reactor design. Int J Hydrogen Energy 2024;59:1376–87. https://doi.org/10.1016/j.ijhydene.2024.02.096.
[33] Geiling J, Steinberger M, Ortner F, Seyfried R, Nuß A, Uhrig F, Lange C, Öchsner R, Wasserscheid P, März M, Preuster P. Combined dynamic operation of PEM fuel cell and continuous dehydrogenation of perhydro-dibenzyltoluene. Int J Hydrogen Energy 2021;46:35662–77. https://doi.org/10.1016/j.ijhydene.2021.08.034.
[34] Preuster P. Entwicklung eines Reaktors zur Dehydrierung chemischer Wasserstoffträger als Bestandteil eines dezentralen, stationären Energiespeichers: Dissertation. FAU Erlangen-Nürnberg; 2017.
[35] Clariant-International-Ltd. EleMax® series – catalyst for storage of hydrogen from renewable sources via liquid organic hydrogen carriers (LOHC). https://www.clariant.com/en/Solutions/Products/2019/05/21/15/19/EleMax-Series. [Accessed 13 July 2024].
[36] Wagner L. LOHC-Speichersystem für die stationäre Wasserstoffpeicherung im 25 kW-Maßstab. Friedrich-Alexander Universität Erlangen-Nürnberg; 2020. Dissertation.
[37] Thomeo JC, Freire JT. Heat transfer in fixed bed: a model non-linearity approach. Chem Eng Sci 2000:2329–38. https://doi.org/10.1016/S0009-2509(99)00465-0.
[38] Thoméo JC, Rouiller CO, Freire JT. Experimental analysis of heat transfer in packed beds with air flow. Ind Eng Chem Res 2004;43:4140–8. https://doi.org/10.1021/ie030759u.
[39] Sosna B, Dong Y, Chromow L, Korup O, Horn R. Effective axial thermal conductivity in catalyst packings from high resolution temperature profiles. Chem Ing Tech 2016;88:1676–83. https://doi.org/10.1002/cite.201600062.
[40] Dong Y, Sosna B, Rosowski F, Horn R. Investigation of radial heat transfer in a fixed-bed reactor: CFD simulations and profile measurements. Chem Eng J 2017: 204–14. https://doi.org/10.1016/j.cej.2017.02.063.
[41] Grattan K, Sun T. Fiber optic sensor technology: an overview. Sensor Actuator 2000:40–61. https://doi.org/10.1016/S0924-4247(99)00368-4.
[42] Stegehake C, Grünewald M, Zanthoff H-W, Hecht C. Fiber-optic temperature measurements in fixed-bed reactors for model-based evaluation of effective radial thermal conductivity. Chem Ing Tech 2018;90:602–14. https://doi.org/10.1002/cite.201700158.
[43] Dong Y, Geske M, Korup O, Ellenfeld N, Rosowski F, Dobner C, Horn R. What happens in a catalytic fixed-bed reactor for n-butane oxidation to maleic anhydride? Insights from spatial profile measurements an particle resolve CFD simulations. Chem Eng J 2018:799–811. https://doi.org/10.1016/j.cej.2018.05.192.
[44] Livio D, Diehm C, Donazzi A, Beretta A, Deutschmann O. Catalytic partial oxidation of ethanol over Rh/Al2O3: spatially resolved temperature and concentration profiles. Appl Catal 2013. https://doi.org/10.1016/j.apcata.2013.07.054.
[45] Horn R, Williams KA, Degenstein NJ, Bitsch-Larsen A, Dalle Nogare D, Tupy SA, Schmidt LD. Methane catalytic partial oxidation on autothermal Rh and Pt foam catalysts: oxidation and reforming zones, transport effects, and approach to thermodynamic equilibrium. J Catal 2007;249:380–93. https://doi.org/10.1016/j.jcat.2007.05.011.
[46] Rüde T, Dürr S, Preuster P, Wolf M, Wasserscheid P. Benzyltoluene/perhydro benzyltoluene – pushing the performance limits of pure hydrocarbon liquid organic hydrogen carrier (LOHC) systems. Sustain Energy Fuels 2022;6:1541–53. https://doi.org/10.1039/D1SE01767E.
[47] Do G, Preuster P, Aslam R, Bösmann A, Müller K, Arlt W, Wasserscheid P. Hydrogenation of the liquid organic hydrogen carrier compound dibenzyltoluene – reaction pathway determination by 1 H NMR spectroscopy. React Chem Eng 2016; 1:313–20. https://doi.org/10.1039/C5RE00080G.
[48] Hydrogenious LOHC Technologies GmbH. EG-Sicherheitsdatenblatt: Reaktionsprodukt der Hydierung und Dehydrierung von Benzyltoluol und Perhydrobenzyltoluol. 2023.
[49] Sasol Germany GmbH. EG-Sicherheitsdatenblatt MARLOHC. 2016.
[50] Iordanidis AA. Mathematical modeling of catalytic fixed bed reactors. Dissertation: University of Twente; 2002.
[51] Roetzel W, Spang B. Overall heat transfer. In: VDI heat Atlas; 2020. p. 67–74.
[52] Müller K, Aslam R, Fischer A, Stark K, Wasserscheid P, Arlt W. Experimental assessment of the degree of hydrogen loading for the dibenzyl toluene based LOHC system. Int J Hydrogen Energy 2016;41:22097–103. https://doi.org/10.1016/j.ijhydene.2016.09.196.
[53] Stein S BR. Structures and properties group additivity model. NIST chemistry WebBook, NIST standard reference database 2009;69:20899.
[54] Jorschick H, Dürr S, Preuster P, Bösmann A, Wasserscheid P. Operational stability of a LOHC-based hot pressure swing reactor for hydrogen storage. Energ Tech 2019;7:146–52. https://doi.org/10.1002/ente.201800499.
[55] Willer M, Preuster P, Wasserscheid P. Dataset of a heat transfer analysis in the continuous reactor for the dehydrogenation of perhydro benzyltoluene and perhydro dibenzyltoluene. Zenodo; 2024. https://doi.org/10.5281/zenodo.12549525.
[56] Wunsch A, Berg T, Pfeifer P. Hydrogen production from the LOHC perhydro-dibenzyl-toluene and purification using a 5 μm PdAg-membrane in a coupled microstructured system. Materials 2020;13. https://doi.org/10.3390/ma13020277.